ISSN 1063-7834, Physics of the Solid State, 2021, Vol. 63, No. 7, pp. 1069–1080. © Pleiades Publishing, Ltd., 2021.
ISSN 1063-7834, Physics of the Solid State, 2021. © Pleiades Publishing, Ltd., 2021.
Russian Text © The Author(s), 2021, published in Fizika Tverdogo Tela, 2021, Vol. 63, No. 7, pp. 854–865.

Universal Behavior and Temperature Evolution of the Magnetoresistance Hysteresis in Granular High-Temperature Superconductors Y–Ba–Cu–O

S. V. Semenov[a, b, *], D. A. Balaev[a, b], and M. I. Petrov[a]

[a] *Kirensky Institute of Physics, Krasnoyarsk Scientific Center, Siberian Branch, Russian Academy of Sciences, Krasnoyarsk, 660036 Russia*

[b] *Siberian Federal University, Krasnoyarsk, 660041 Russia*

**e-mail: svsemenov@iph.krasn.ru*

Received March 17, 2021; revised March 17, 2021; accepted March 22, 2021

Abstract—Regularities in the behavior of the magnetoresistance hysteresis $R(H)$ in the granular yttrium high-temperature superconductors (HTSs) have been established. For this purpose, a comparative analysis of the magnetotransport properties has been carried out on the granular HTS samples, which exhibit (i) approximately the same magnetic properties and temperatures of the onset of the superconducting transition (90.5–93.5 K, which is characteristic of HTS grains) and (ii) different critical transport currents J_C (which is characteristic of grain boundaries). Despite a significant (by more than an order of magnitude) spread of the J_C values for the three samples, a universal behavior of the magnetoresistance hysteresis has been found, which is apparently inherent in all the granular Y–Ba–Cu–O compounds. The $R(H)$ hysteresis is extremely broad and, in a fairly wide external field range, the dependence of the magnetoresistance hysteresis width ΔH on the field H_{dec} (the external field for the decreasing hysteresis branch is $H = H_{dec}$) is almost linear: $\Delta H \approx H_{dec}$. This behavior is observed over the entire temperature range of implementation of the superconducting state (the investigations have been carried out at temperatures of 77–88 and 4.2 K). The result obtained has been explained by considering the effective field in grain boundaries, which is a superposition of the external field and the field induced by the magnetic moments of grains. The field induced by grains, in turn, significantly increases in the region of grain boundaries due to the magnetic flux compression (the grain boundary length is shorter than the HTS grain size by several orders of magnitude). The aforesaid has been confirmed by the analysis of the $R(H)$ hysteresis for the Y–Ba–Cu–O- and CuO-based HTS composite, in which the grain boundary length is purposefully increased; as a result, the flux compression is less pronounced and the $R(H)$ hysteresis narrows.

Keywords: granular HTS, magnetoresistance hysteresis, grain boundaries

DOI: 10.1134/S1063783421070192

1. INTRODUCTION

It is well known that polycrystalline (hereinafter, granular) high-temperature superconductors (HTSs) are two-level superconducting systems in their transport and magnetotransport properties. HTS grains are characterized by fairly high critical current densities (the so-called intragrain critical current J_{CM}) and it is the intragrain currents that determine the magnetic response of bulk samples in moderate and strong magnetic fields. At the same time, the existence of grain boundaries with a thickness of no more than few nanometers already significantly (by several orders of magnitude) decreases the critical density of the transport current in bulk samples. This is due to the fact that the thickness or geometric length of grain boundaries is comparable with the HTS coherence length and, as a result, the superconducting current transport through grain boundaries occurs via Josephson tunneling, in which the critical current is much lower. The aforesaid can be considered to be the basis for applicability of the concept of a two-level (grains and boundaries) superconducting system [1] to the description of the magnetic and transport properties of granular HTSs. In this case, the strict inequality $J_{CM} \gg J_C$ is obvious, where J_C is the critical transport current. For a long time since the discovery of HTS materials, many regularities in the effect of different factors on the morphology of grain boundaries and, ultimately, on the behavior of transport characteristics have been established [2–10]. To describe the dissipation processes in the subsystem of grain boundaries, one can use the standard approaches developed for type-II superconductors [10–23]. Note that, despite a great number of studies on the description of dissipation

processes in granular HTS systems [10–24], bright features in the behavior of the electrical resistance in external fields have been recently found that indicate the occurrence of a topological (Berezinskii–Kosterlitz–Thouless) phase transition in the intergrain medium [25–28].

However, if we consider already the magnetotransport characteristics of granular HTSs (magnetoresistance $R(H)$ and critical transport current $J_C(H)$ as functions of the external field), then, to understand most effects, it is necessary to take into account the interaction between these superconducting subsystems. Indeed, there is a set of experimental facts that cannot be explained in the framework of the conventional approach. These facts include the following:

(i) A fairly complex shape of the $R(H)$ hysteresis [29–42] and $J_C(H)$ [43–47]; in this case, we have $R(H_{inc}) > R(H_{dec})$ and $J_C(H_{inc}) < J_C(H_{dec})$ under cycling of the external field to some constant value $\pm H_{max}$ (hereinafter, the subscripts inc and dec are referred to the increasing and decreasing external fields, respectively), although, in the initial magnetoresistance branch $R(H_{ini})$ in relatively weak external field, the situation is opposite: $R(H_{ini}) < R(H_{dec})$.

(ii) A nonmonotonic behavior of the $R(H_{inc})$ (a local maximum is often observed) and $R(H_{dec})$ dependences (there is a minimum or the resistance becomes zero) [29, 31–33, 36–39, 42].

(iii) The magnetoresistance anisotropy with respect to the mutual orientation of the external field and macroscopic transport current **j**; in this case, we have $R(\mathbf{H} \parallel \mathbf{j}) < R(\mathbf{H} \perp \mathbf{j})$ [36, 37, 48–52] and the $R(H)$ hysteresis is broader at the perpendicular orientation $\mathbf{H} \perp \mathbf{j}$ [53–55].

(iv) The effect of thermomagnetic prehistory on the $R(T)$ dependence: the conditions of cooling in external field H ensure the weaker dissipation than the conditions of zero field cooling with subsequent applying external field H of the same value [46, 48, 49, 54, 56–62].

(v) An extremely broad magnetoresistance hysteresis, i.e., a large ΔH value determined as $\Delta H = H_{dec} - H_{inc}$ under the condition $R(H_{dec}) = R(H_{inc})$.

The set of above-listed facts (i)–(v) is qualitatively explained by considering an effective field in the intergrain medium [63, 64]. Here, of fundamental importance is the interaction between the subsystems of grains and grain boundaries, at which the magnetic moments $\mathbf{M}_G$ of HTS grains induce the field in grain boundaries (Fig. 1). As a result, the subsystem of grain boundaries is in the effective field $\mathbf{B}_{eff}$, which is a superposition of external field **H** and field $\mathbf{B}_{ind}$ induced by grains in the intergrain medium. The magnetic response of HTS grains is determined by both the Meissner currents (in the critical state model, the current with the critical density circulates) and Abrikosov vortices captured by grains. Taking into account the hysteretic field dependence of the magnetization $M(H)$ and the direction of the induced field $\mathbf{B}_{ind}$ (Fig. 1), the equation for the effective field

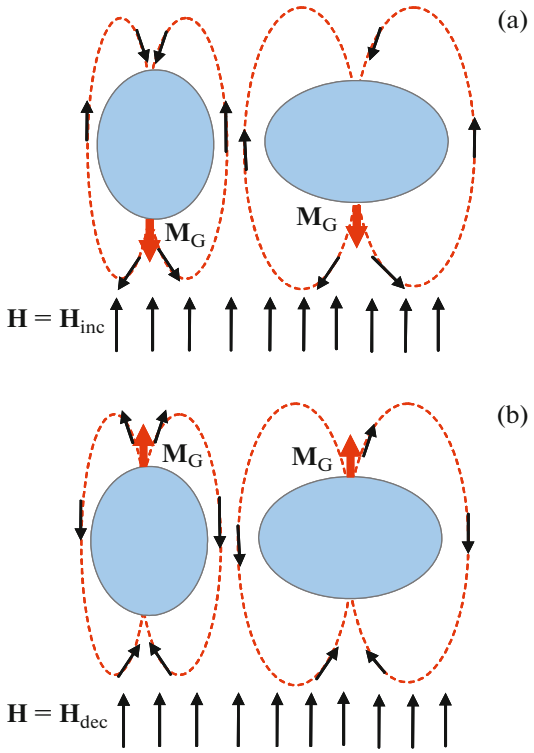

Fig. 1. Schematic of directions of the lines of magnetic induction $\mathbf{B}_{ind}$ from magnetic moments $\mathbf{M}_G$ (the $\mathbf{M}_G$ direction is determined by a sign of magnetization M of the sample) of HTS grains (ovals) in the intergrain medium (in this representation, the spacings between grains are strongly enlarged). (a, b) Increasing ($\mathbf{H} = \mathbf{H}_{inc}$) and decreasing ($\mathbf{H} = \mathbf{H}_{dec}$) fields. (a) $\mathbf{B}_{ind} \parallel \mathbf{H}$; (b) the magnetic induction lines are directed oppositely to the external field.

$$B_{eff}(H) = |H - 4\pi M(H)\alpha| \quad (1)$$

is valid in the intergrain medium. The absolute value was used in Eq. (1) because the sign of the resulting effective field is unimportant in describing the dissipation processes and the magnetoresistance R is a function of B_{eff}: $R = f(B_{eff})$. The factor α in Eq. (1) includes the averaged demagnetizing factor and the degree of flux compression in the intergrain spacings. The description of the experimental data on the magnetoresistance hysteresis $R(H)$ of granular HTSs using Eq. (1) yielded good qualitative [54, 55, 65–69] and quantitative [70] agreement. However, this agreement is achieved if it is only assumed that the α value is about 20–25 (for the perpendicular orientation $\mathbf{H} \perp \mathbf{j}$). This proves the stronger flux compression in the intergrain medium as compared with the HTS grain size (micrometers); the possibility of implementation of such a magnetic flux compression was first mentioned in [52].

Table 1. Critical transport current J_C, resistivity ρ, intragrain ("magnetic") critical current J_{CM} (Eq. (3)), average grain size $\langle d \rangle$, and physical density of the samples

Sample	J_C (77 K) A/cm^2	J_C (4.2 K) A/cm^2	ρ (95 K) mΩ cm^2	J_{CM} (77 K) A/cm^2	J_{CM} (4.2 K) A/cm^2	$\langle d \rangle$ μm	Density, % theor.
YBCO-1	150	1500	0.45	2×10^5	5.5×10^6	10	93
YBCO-2	15	170	2.2	5.6×10^5	7.4×10^6	5	86
YBCO-3	5	100	6	1.5×10^5	2.3×10^6	4	88
YBCO-comp	<0.01	0.1	800	3×10^5	8×10^6	2	~60

In the approach commonly used to describe the dissipation of type-II superconductors, the dependence of the magnetoresistance on external field H, temperature T, and transport current I is determined by the dependence of the pinning potential $U_P(H, T, I)$ on these parameters through the Arrhenius equation $R(H, T, I) = R_N \exp(-U_P(H, T, I)/kT)$ [71], where R_N is the resistance in the normal state. For the grain boundaries or the Josephson medium, it is reasonable to use the term Josephson coupling energy $E_J(H, T, I)$ instead of $U_P(H, T, I)$ and, according to Eq. (1), to use already the effective field $B_{eff}(H)$ instead of the external field H [70]:

$$R(H,T,I) = R(B_{eff}(H),T,I) = R_N \exp(-E_J(B_{eff}(H),T,I)/kT). \quad (2)$$

It is clear that the $E_J(B_{eff}(H), T, I)$ dependence is determined by many factors, including the average thickness of grain boundaries, their type (metallic or insulating), etc. Obviously, these factors depend on the conditions of synthesis and final heat treatment of the HTS materials and, here, it is reasonable to expect a completely different behavior of the magnetoresistance and its temperature evolution for the HTS samples prepared by different methods. In this study, however, we show that the temperature evolution of the magnetoresistance hysteresis is universal for the samples with different current-carrying capacities. This is demonstrated by the example of the $YBa_2Cu_3O_7$ system for three samples synthesized under different conditions and having different critical currents. The indicated universal behavior is no longer observed in the HTS composite in which the addition of a nonsuperconducting component further reduces the energy of the Josephson coupling (and, hence, the critical current) due to an increase in the grain boundary length. The results obtained are closely related to the effect of the magnetic flux compression in the intergrain medium.

2. EXPERIMENTAL

The investigated $YBa_2Cu_3O_7$ HTS samples were prepared by the solid-state synthesis with 3–5 intermediate grindings. For the sample with the highest critical current density (sample YBCO-1), the final annealing stage was performed at a temperature of ~940°C close to the melting point for 50 h. Upon completion of the synthesis, the sample was annealed at a temperature of 350°C for 10 h to reach the oxygen stoichiometry. For samples YBCO-2 and YBCO-3, the total annealing time was 160 h at temperatures of 920–930°C; at the end of the synthesis, the samples were annealed at a temperature of 300°C for 3 h and slowly cooled together with a furnace to room temperature for oxygenation. According to the X-ray diffractometry data, all the peaks for the obtained samples belong to the structure 1–2–3 and no side reflections are observed.

The composite sample (hereinafter, YBCO-comp) containing 77.5 vol % of the $Y_{0.75}Lu_{0.25}Ba_2Cu_3O_7$ superconductor and 22.5 vol % of copper oxide CuO was prepared by fast backing technique [53, 72]. In this method, the $Y_{0.75}Lu_{0.25}Ba_2Cu_3O_7$ HTS preliminary prepared by the solid-state synthesis and characterized was used, which was milled in a powder and added with the reagent CuO of special purity grade in a required ratio. After joint grinding of the components and pressing, the obtained tablet was placed in a furnace preheated to 915°C for 5 min; after that, the sample was moved to another furnace heated to 350°C for annealing for 4 h followed by cooling in the furnace for oxygenation. According to the X-ray diffraction data, all the peaks of the obtained composite sample belong to the 1–2–3 structure and copper oxide; no foreign reflections were observed.

The data on the physical density determined by weighing the samples in alcohol and the average superconductor grain size determined from scanning electron microscopy images obtained on a Hitachi-TM 3000 microscope are given in Table 1.

The magnetotransport measurements were performed by a four-point method. Samples about 0.15–0.15–7 mm^3 (±50%) in size were cut from the tablets and the transport current I co-directed with the long sample axis was applied. Gold-plated clamp contacts were used. The critical current was determined according to the criterion 1 μV/cm; the sample was immersed in liquid nitrogen or liquid helium. The external field was set by an electromagnet in measur-

ing the magnetoresistance $R(H)$ at high temperatures (from 77 K) and by a superconducting solenoid in measuring $R(H)$ at $T = 4.2$ K. The $R(H)$ dependences for the YBCO samples measured at 4.2 and 77 K and a transport current of ~30 mA or stronger were obtained by placing the sample directly in liquid helium or liquid nitrogen, respectively, to avoid heating on the current contacts. When measuring the $R(T)$ and $R(H)$ dependences at weak (up to 10 mA) measuring currents, the sample was placed in a heat-exchange helium medium. Some of the $R(T)$ and $R(H)$ measurements were performed on a PPMS-6000 system. In all the cases, the sample was cooled in zero external field and the external field was perpendicular to the current direction: $\mathbf{H} \perp \mathbf{I}$.

The magnetic properties were investigated on a vibrating sample magnetometer under the external conditions (including the external magnetic field sweep rate) corresponding to the magnetotransport measurements.

3. RESULTS AND DISCUSSION

3.1. Intragrain and Intergrain Critical Current and Resistive Transition

According to the magnetic measurement data, the temperatures of the onset of the diamagnetic signal from the magnetic measurements were 93, 92.5, 90.5, and 93.5 K for samples YBCO-1, YBCO-2, YBCO-3, and YBCO-comp, respectively. At the same temperatures, the onset of a resistive transition (a sharp decrease in the resistance) is observed. Table 1 gives the data on the critical current density J_C of the investigated samples. The J_C value for sample YBCO-1 is very high at both helium and nitrogen temperatures. During the synthesis of samples YBCO-2 and YBCO-3, no special measures were taken to obtain the high J_C values and it can be seen that the critical current in these samples is significantly (by an order of magnitude) lower. At the same time, the electrical resistivity ρ in the normal (95 K) state also increases (see Table 1) and there is the correlation with the physical density. In the HTS composites prepared by fast backing technique, the nonsuperconducting component acts as grain boundaries [53, 72] and the introduction of an insulator [14, 53, 72] leads to additional weakening of the Josephson coupling and, consequently, to the very low J_C values and high resistivity in the normal state.

Figure 2 shows the magnetic hysteresis loops for the investigated samples at temperatures of 77 K (Fig. 2a) and 4.2 K (Fig. 2b). At $T = 4.2$ K, the $M(H)$ dependences are almost symmetric relative to the abscissa axis, while at 77 K this is no longer observed (see the left-hand inset in Fig. 2a). The occurrence of the asymmetry at high temperatures is related to weakening of the Abrikosov vortex pinning in the surface layer of grains [73, 74]. The absolute values of the magnetization (in a certain field) of the samples are somewhat different. Using the magnetization values of the full hysteresis loop, we can determine the intragrain critical current density J_{CM} [75]. According to the expression following from the Bean's model, we have

$$J_{CG}\ (\mathrm{A/cm^2}) = 30\Delta M\ (\mathrm{emu/cm^3})/d\ (\mathrm{cm}), \quad (3)$$

where d is the average grain size and $\Delta M = M(H_{inc}) - M(H_{dec})$ at $H_{inc} = H_{dec}$. The J_{CM} values in an external field of $H \sim 100$ Oe obtained using Eq. (3) are given in Table 1. It can be seen that the J_{CM} values for a series of the investigated samples are of the same order of magnitude. Note that, comparing the data on the critical transport current J_C and the "magnetic" (intragrain) critical current J_{CM}, we can make certain of the validity of the strict inequality $J_{CM} \gg J_C$, which follows from the concept of a two-level superconducting system in granular HTSs.

The difference between the densities of the critical transport current J_C (Table 1) of the investigated samples or, in fact, between the energies of the Josephson coupling, manifests itself also in the degree of broadening of the superconducting transition under the action of an external magnetic field and transport current. Figure 3 presents the $R(T)$ dependences for the selected samples: YBCO-2 (Fig. 3a) and YBCO-comp (Fig. 3b) in different external fields at two current values. The two-step $R(T)$ dependences in Fig. 3 reflect the presence of two superconducting subsystems [2, 12–14, 21–23, 47, 52–54, 60, 62, 76–78]; a sharp jump in the resistance corresponds to the superconducting transition in HTS grains and the extended $R(T)$ tail reflects the dissipation processes in the subsystem of grain boundaries. The value of the smooth portion of the $R(T)$ dependences for different H and I values near the beginning of their divergence (after the transition in grains) corresponds to the total or "normal" resistance (analogue of R_N in Eq. (2)) of the subsystem of grain boundaries hereinafter referred to as R_{NGB}. The magnetic field range for the data in Fig. 3 (up to 5–8 kOe) is sufficiently small to cause a noticeable broadening of the superconducting transition in grains; however, in the subsystem of grain boundaries, the broadening of the resistive transition to some temperature T_{C0} (the state $R = 0$) manifests itself already in sufficiently weak external fields. In addition, it can be seen in Fig. 3 that a tenfold increase in the transport current also broadens the resistive transition. The comparison of the degrees of broadening of the resistive transition in samples YBCO-2 and YBCO-comp (the external current fields in Figs. 3a and 3b are approximately the same) shows that the grain boundaries in the composite are significantly deteriorated by the incorporation of CuO.

Figure 4 shows field dependences of the temperature T_{C0} for the investigated samples in the logarithmic

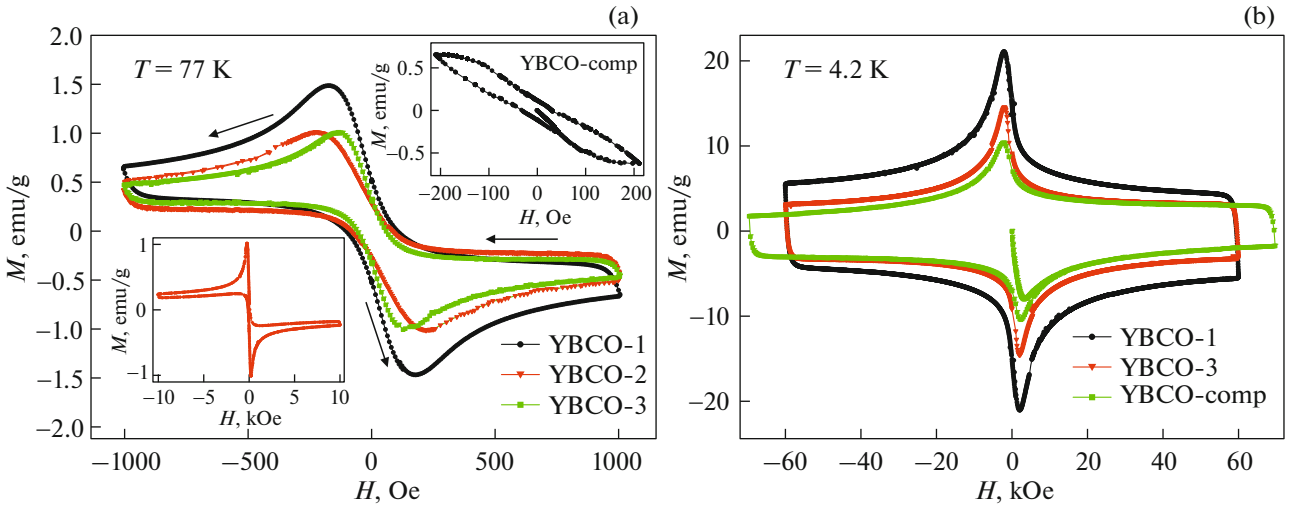

Fig. 2. Magnetic hysteresis loops $M(H)$ for the investigated samples at T = (a) 77 and (b) 4.2 K. (a) Left-hand inset: $M(H)$ for sample YBCO-2 up to the maximum applied field of $|H_{max}| = 10$ kOe. Right-hand inset: $M(H)$ for sample YBCO-comp. Arrows show the direction of the change (increase or decrease) in the external field H.

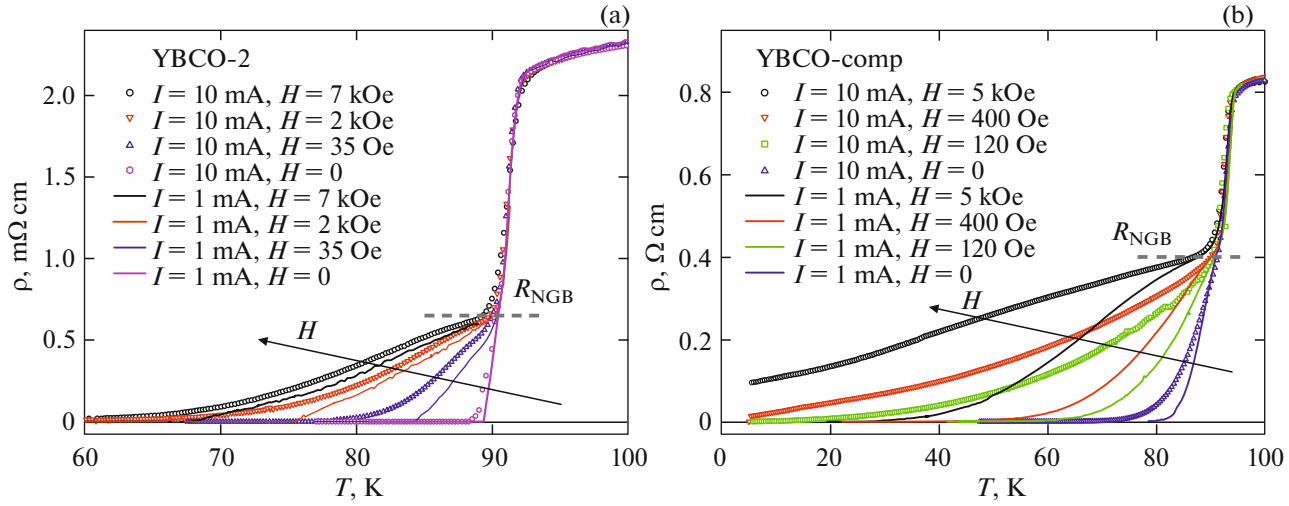

Fig. 3. $R(T)$ dependences for samples (a) YBCO-2 and (b) YBCO-comp at the indicated external fields H and transport currents I (the current densities at the same I value are approximately the same for the two samples). The normal resistance R_{NGB} of the subsystem of grain boundaries is indicated.

scale. Note that these data were obtained at approximately the same transport current densities (the transport current is $I = 1$ mA) and, taking into account the similarity of the temperatures of the onset of the superconducting transition in all the samples, we can assume that the degree of a decrease in T_{C0} with increasing field is inversely proportional to the energy of the Josephson coupling. The analysis of the data on J_C (Table 1) and $T_{C0}(H)$ dependence (Fig. 4) shows that, for a series of samples YBCO-1, YBCO-2, YBCO-3, and YBCO-comp, the grain boundaries gradually deteriorate in terms of transparency for superconducting current carriers. At the same time, the magnetic properties, intragrain critical current, and transition temperature of HTS grains are approximately the same.

3.2. Magnetoresistance Hysteresis and Its Description

Figure 5 shows typical hysteretic dependences of the magnetoresistance $R(H)$ at sufficiently high (77 K and more) temperatures. The $R(H)$ dependences are normalized to the R_{NGB} value (Fig. 3). Such a representation of the magnetoresistance makes it possible to estimate the degree of the resistive response from grain

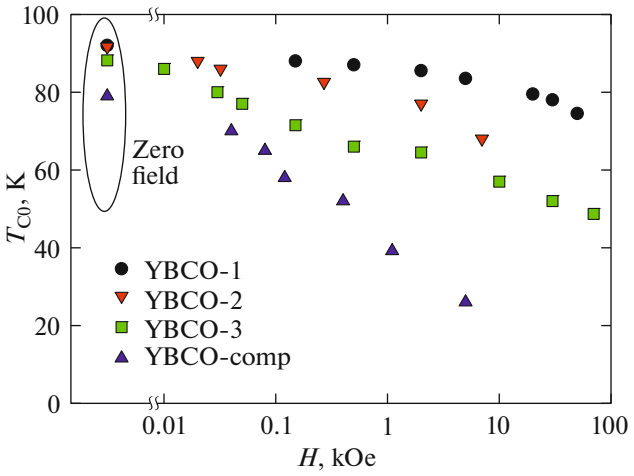

Fig. 4. Dependences of temperature T_{C0} (states $R = 0$, see Fig. 3) on external field H for a series of the investigated samples. The H axis is in the logarithmic scale; the point with $H = 0$ corresponds to 0.5 Oe.

boundaries relative to the maximum possible value (at $R = R_{NGB}$). For samples YBCO-1 and YBCO-3 (Figs. 5a and 5b, respectively), there is a great difference between the R/R_{NGB} values at approximately the same transport currents I. This is caused by the different critical currents of these samples (Table 1).

Figure 5 shows almost the entire variety of the observed types of the $R(H)$ dependences for the granular yttrium HTS systems in the high-temperature region. The character of the hysteretic $R(H)$ dependences was described in Introduction. The data in Fig. 5 obey the inequality $R(H_{inc}) > R(H_{dec})$ in a wide field range. At the same time, the initial branch of the magnetoresistance $R(H_{ini} = H_{inc})$ contains a portion in the field region near $H = 0$ where the situation is opposite: $R(H_{ini}) < R(H_{dec})$, see the left-hand inset in Figs. 5b and 5c. The nonmonotonic behavior of the $R(H_{inc})$ dependence manifests itself as a bright feature for sample YBCO-1 (Fig. 5a). For sample YBCO-3, the local maximum is much weaker (Fig. 5b). According to the results reported in [39, 65–70], the presence of a local maximum in the $R(H_{inc})$ dependence corresponds to the minimum in the $M(H_{inc})$ dependence, since the $M(H)$ dependence enters Eq. (1) for the effective field and the magnetoresistance is a function of B_{eff} (Eq. (2)). The minimum in the reverse course of the magnetoresistance in Fig. 5b and the left-hand inset in it (sample YBCO-3), as well as in Fig. 5c (sample YBCO-comp) corresponds to the situation when the external field is compensated, to the greatest extent, by the field B_{ind} induced by grains (Fig. 1b). For sample YBCO-1, under the experimental conditions in Fig. 5a, a relatively small measuring current is lower than the critical current at the effective field $B_{eff}(H_{dec})$ for the descending field branch; therefore, in the reverse course, the magnetoresistance is $R(H_{dec}) = 0$. The $R(H)$ dependences in Figs. 5a, 5b, and 5c were obtained during cycling for maximum fields H_{max} of no more than ±1 kOe; in stronger fields, the $R(H)$ dependence smoothly approaches the R_{NGB} value, which is shown in the right-hand insets in Figs. 5b and 5d; in this case, in sufficiently strong fields, the hysteresis becomes rather narrow.

The validity of the strict inequality $J_{CM} \gg J_C$ means the absence of dissipation in grains. The onset of dissipation in grains is accompanied by an additional sharp increase in the magnetoresistance in the field H^* corresponding to the zero intragrain critical current $J_{CM}(H^*) = 0$ or the condition $\Delta M(H^*) = 0$ [40, 47, 76, 77]. Figure 5d shows the $R(H)$ dependences for sample YBCO-3 at $T = 77.4$ and 85 K. It can be seen that a fairly sharp change in the $R(H)$ dependence at $T = 85$ K occurs at a resistance value of $R \approx R_{NGB}$ (in this case, the R_{NGB} value was obtained independently of the $R(T)$ curves in different fields). At $T = 85$ K, we have $H^* \approx 20$ kOe and, with decreasing temperature, the characteristic field H^* increases (at $T = 77.4$ K, the H^* value is about 70 kOe). Note that the transport current densities, which can be varied in the experiments, are much lower than J_{CM}; therefore, it is almost impossible to observe a decrease in H^* from the magnetotransport measurements, at least for granular HTSs of the yttrium system.

The hysteretic behavior of $R(H)$ is explained by considering the effective field in the intergrain medium determined by Eq. (1). Simplifying Eq. (2), the magnetoresistance is proportional to the effective field: $R(H) \sim B_{eff}(H)$. We show an example of the qualitative description of the observed $R(H)$ hysteresis form using the sample data as an example. Figure 6a presents the $B_{eff}(H)$ dependences obtained from Eq. (1) using the experimental $M(H)$ data for sample YBCO-1 (Fig. 2a) and different α values. First of all, we should note the similarity of the shapes of the $B_{eff}(H)$ and $R(H)$ hysteresis: the inequality $B_{eff}(H_{inc}) > B_{eff}(H_{dec})$ is valid. It is clear that the experimental magnetization hysteresis enters Eq. (1) in the inverted form and its relative contribution to B_{eff} is determined by the α value. According to the data in Fig. 6a, at an α value of ~10 or more, there is a pronounced maximum in the $B_{eff}(H_{inc})$ dependence corresponding to the maximum in the $R(H_{inc})$ dependence. The minimum in the $B_{eff}(H_{dec})$ dependence is also reproduced within this approach. The effect of flux crowding in itself is expressed in the much stronger effective field B_{eff} in the weak field region than the value of external field H (Fig. 6b). In strong fields, the contribution of the magnetization in Eq. (1) is already insignificant and we have $B_{eff} \approx H$ (Fig. 6b).

In the described approach, the $R(B_{eff})$ dependence is already hysteresisless: $R(B_{eff}(H_{inc})) = R(B_{eff}(H_{dec}))$ at $B_{eff}(H_{inc}) = B_{eff}(H_{dec})$. Therefore, we can operate with

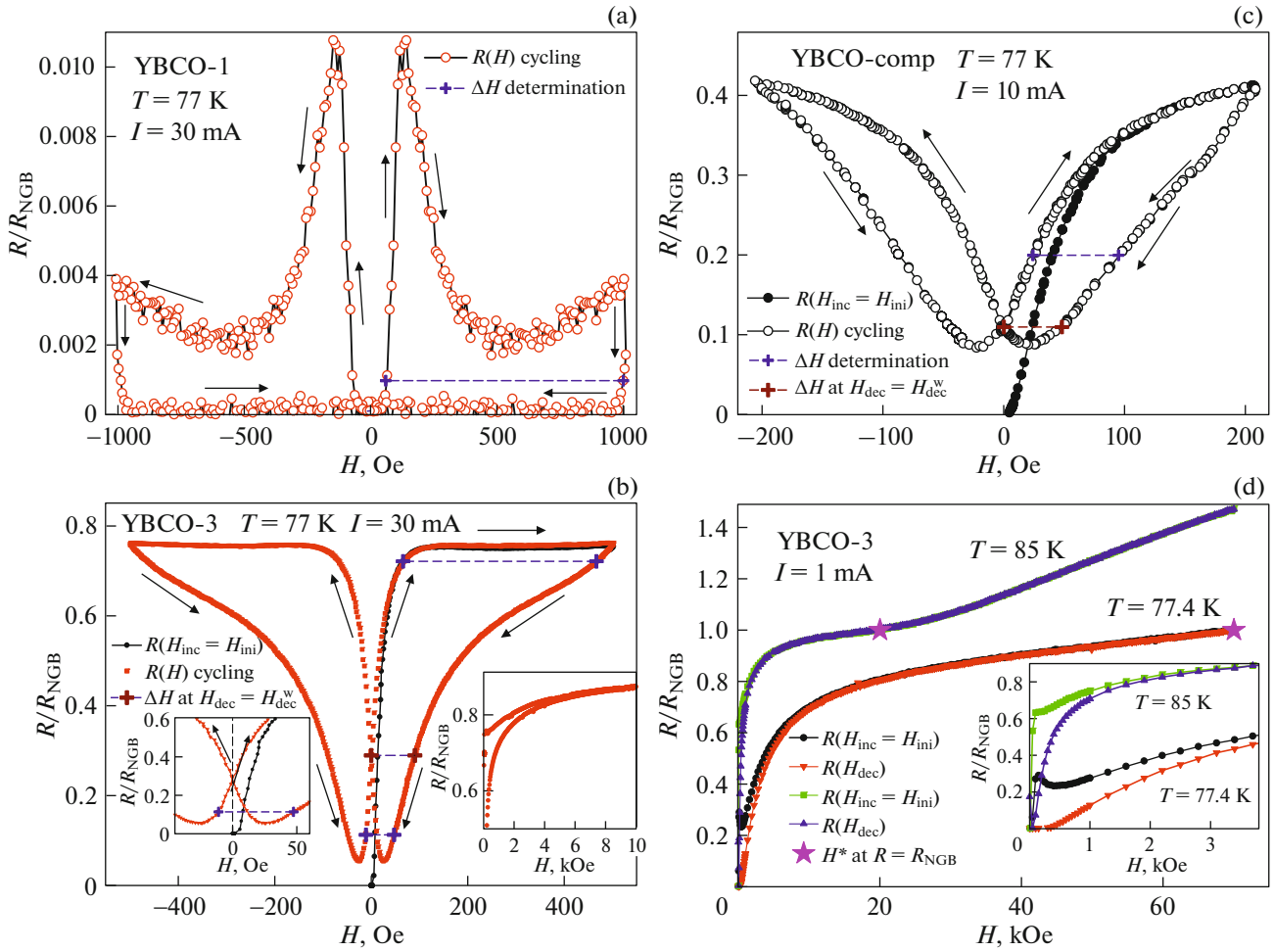

Fig. 5. Typical hysteretic dependences of the magnetoresistance for the investigated samples at relatively high temperatures. The resistance data are normalized to R_{NGB} (Fig. 3). Arrows show the direction of the change in external field H. Both (b, c, d) the initial branches $R(H_{inc} = H_{ini})$ and (a, b, c) the $R(H_{inc})$ and $R(H_{dec})$ dependences are shown upon cycling of the external field to the same $\pm H_{max}$ value. (d) The $R(H)$ dependences (d) contain the initial branches: $R(H_{inc} = H_{ini})$ and the reverse $R(H_{dec})$ course at the indicated temperatures; in addition, the field H^* of the dissipation onset in grains ($R(H^*) \approx R_{NGB}$) is indicated. (a, b, c) The dashed horizontal lines explain the determination of the magnetoresistance hysteresis field width $\Delta H = H_{dec} - H_{inc}$ under the condition $R(H_{dec}) = R(H_{inc})$.

such a characteristic of the $R(H)$ and $B_{eff}(H)$ dependences as the hysteresis field width $\Delta H = H_{dec} - H_{inc}$ under the condition $R(H_{inc}) = R(H_{dec})$ or $B_{eff}(H_{inc}) = B_{eff}(H_{dec})$. It was previously shown that, for the hysteretic $R(H)$ dependences of granular HTSs, the ΔH value is independent of the transport current in a fairly wide current range [47, 61, 63, 64, 67, 69]. Consequently, even the qualitative description of the $R(H)$ hysteresis requires the consistency between the ΔH values obtained from the experimental $R(H)$ and ΔH dependences and reproduced by the $B_{eff}(H)$ dependence. The $R(H)$ hysteresis in fields of up to $H_{max} \sim \pm 1$ kOe is fairly wide (Figs. 5a and 5b) and, in order to reproduce the similar ΔH values of the $B_{eff}(H)$ dependence, the parameter α should range between 20–25. As for the data in a wider field range, here the $R(H)$ hysteresis becomes narrow (the right-hand inset in Figs. 5b and 5d); in this field range, the magnetization hysteresis is fairly small (the left-hand inset in Fig. 2b) and, consequently, the $B_{eff}(H)$ hysteresis is also narrow (Fig. 6b). Note that, for the better and more detailed description of the $R(H)$ hysteresis, the parameter α should be considered as a function of the external field.

At low temperatures (4.2 K), the character of the $R(H)$ hysteresis remains the same: $R(H_{inc}) > R(H_{dec})$, as can be seen in Fig. 7, which shows the $R(H)$ dependences for samples YBCO-1 and YBCO-3. To measure the magnetoresistance at low temperatures, the significantly higher transport current densities than at high temperatures are required. In this case, the external field range corresponding to the broad $R(H)$ hys-

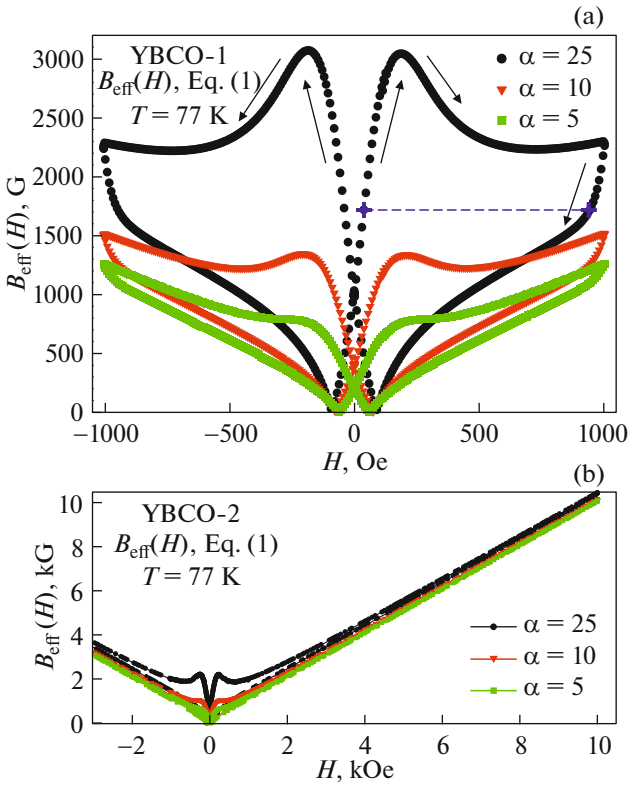

Fig. 6. Hysteretic dependences of the effective field $B_{eff}(H)$ at $T = 77$ K plotted according to Eq. (2) at different α values (indicated) using the magnetization data (Fig. 2) for samples (a) YBCO-1 at $|H_{max}| = 1$ kOe and (b) YBCO-2 at $|H_{max}| = 10$ kOe. Arrows show the direction of the change in external field H. (a) The dashed horizontal line explains the determination of the hysteresis field width of the effective field $\Delta H = H_{dec} - H_{inc}$ under the condition $B_{eff}(H_{dec}) = B_{eff}(H_{inc})$.

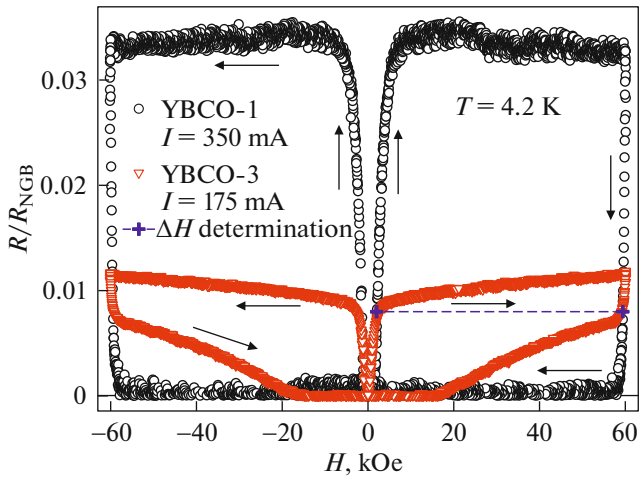

Fig. 7. Hysteretic $R(H)$ dependences for samples YBCO-1 and YBCO-3 at $T = 4.2$ K obtained upon cycling of the external field up to ±60 kOe. The resistance data are normalized to R_{NGB} (see Fig. 3). Arrows show the direction of the change in external field H. The dashed horizontal line explains the determination of the magnetoresistance hysteresis field width $\Delta H = H_{dec} - H_{inc}$ under the condition $R(H_{dec}) = R(H_{inc})$.

teresis also increases. This is consistent with the explanation using Eq. (1) with allowance for the fact that the absolute values of the magnetization also increased by more than an order of magnitude (Fig. 2b); i.e., the effective fields for the forward and reverse branches are also strongly different. It is noteworthy that the $R(H_{inc})$ dependences have no pronounced maxima, although, in contrast to the data in Fig. 5b, the R/R_{NGB} values are far from their maximum value.[1] The possible reasons for the absence of a pronounced maximum, which corresponds to the minimum in the $M(H)$ dependence (Fig. 2b) and, according to Eq. (1), is expected in the region of ~2 kOe, were discussed in [69]. For the composite sample, the form of the $R(H)$ hysteresis and the relative position of the initial branch of the magnetoresistance $R(H_{ini} = H_{inc})$ and the $R(H_{inc})$ and $R(H_{dec})$ dependences at low temperatures (Fig. 8) remain the same as for the high-temperature data.

[1] If the grain boundaries have a metallic conductivity [3, 6], one may expect a decrease in R_{NGB} with temperature, which will lead to the somewhat higher R_{NGB} value for the data in Fig. 7.

3.3. Universal Behavior of the R(H) Hysteresis Width

Let us analyze the behavior of the magnetoresistance hysteresis width $\Delta H = H_{dec} - H_{inc}$ (at $R(H_{dec}) = R(H_{inc})$) for different samples at different temperatures. We consider the total $R(H)$ hysteresis loop obtained under cycling of the external field (without the initial course of $R(H_{ini} = H_{inc})$). The $R(H)$ hysteresis width is, in fact, the length of a horizontal segment between points of the decreasing $R(H_{dec})$ and increasing $R(H_{inc})$ branches of the magnetoresistance hysteresis. Typical examples of determining the ΔH value are shown in Figs. 5a, 5b, 5c, 7, and 8a (dashed horizontal lines). The ΔH value must always be less than the H_{dec} value until, in some field H_{dec}^{w}, the resistance value $R(H_{dec} = H_{dec}^{w})$ becomes equal to $R(H_{inc} = 0)$. Then, unambiguously, we have $\Delta H(H_{dec} = H_{dec}^{w}) = H_{dec}$ (see Figs. 5b, 5c, 8b). In the range $0 \le H < H_{dec}^{w}$, ΔH will already be larger than the H_{dec} value. The H_{dec}^{w} field value does not exceed 50–60 Oe for the high-temperature data (Figs. 5b, 5c) and 10 kOe at 4.2 K for sample YBCO-comp (Fig. 8b), which is much lower than the maximum field H_{max}. Note that, in a certain range $H < H_{dec}$, the resistance is zero (see Figs. 5a and 7), while here the ΔH value is undetermined.

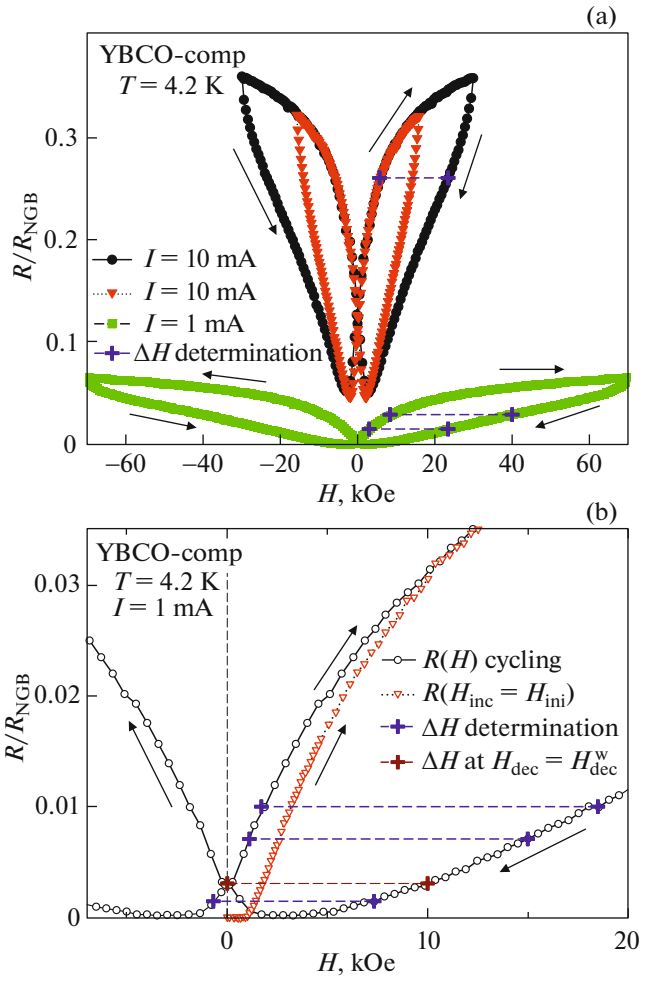

Fig. 8. Hysteretic $R(H)$ dependences for sample YBCO-comp at $T = 4.2$ K obtained at different transport currents (indicated) upon field cycling to different H_{max} values. (b) Relative positioning of the initial magnetoresistance branch $R(H_{inc})$ and $R(H)$ upon cycling of the external field. The resistance data are normalized to the R_{NGB} value (see Fig. 3). Arrows show the direction of the change in external field H. Dashed horizontal lines explain the determination of the magnetoresistance hysteresis field width $\Delta H = H_{dec} - H_{inc}$ under the condition $R(H_{dec}) = R(H_{inc})$.

Figure 9 shows the $\Delta H(H_{dec})$ dependences obtained from the experimental $R(H)$ data at different temperatures for samples YBCO-1, YBCO-2, and YBCO-3. A double logarithmic scale is used due to the different ranges of the maximum applied field at low (10–60 kOe) and high (1–10 kOe) temperatures. For the high-temperature data, in fields H_{dec} above ~1 kOe, as was mentioned in the discussion of the $R(H)$ hysteresis (see Subsection 3.2), the ΔH values are small (see the data for sample YBCO-2 at $T = 77$ K) and the inequality $\Delta H\,(H_{dec} = H^{w}_{dec}) > H_{dec}$ is met in the field range of $0 \le H < H^{m}_{dec}$. In addition, for sample YBCO-1, the

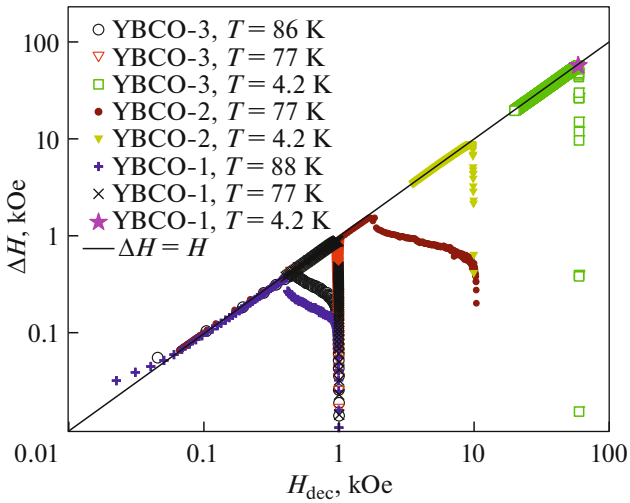

Fig. 9. Magnetoresistance hysteresis field width ΔH versus field H_{dec} (a double logarithmic scale was used) for samples YBCO-1, YBCO-2, and YBCO-3 (symbols) at the indicated temperatures and different H_{max} values. The solid line shows the linear dependence $\Delta H = H_{dec}$.

magnetoresistance in the reverse course drops to zero almost stepwise (Fig. 7) and the $\Delta H(H_{dec})$ dependence contains, literally, one point shown in Fig. 9.

The main thing that attracts attention in Fig. 9 is the closeness of the obtained experimental $\Delta H(H_{dec})$ data to the linear function $\Delta H = H$ (solid line in Fig. 9a) in a wide range of the field H_{dec} and the identity of the $\Delta H(H_{dec})$ dependences for different samples at different temperatures. Following the dependence $\Delta H \approx H_{dec}$ means that the $R(H_{inc})$ dependence increases fairly fast and, upon reaching a certain field H^{m}_{inc}, turns to the weak field dependence; then, if H^{m}_{inc} is sufficiently small as compared with H_{max}, it is logical that $\Delta H \approx H_{dec}$. It was found quite unexpectedly that, despite the large differences in the critical transport currents (Table 1), magnetotransport properties (Fig. 3), and shapes of the $R(H)$ dependences (Figs. 5, 7), all the yttrium HTS samples under study exhibit a certain universal behavior of the magnetoresistance hysteresis at different temperatures.

The $R(H)$ hysteresis width should coincide with the width of the hysteresis of the effective field $B_{eff}(H)$. Substituting sequentially $H = H_{inc}$ and $H = H_{dec}$ into (1) and subtracting the obtained expressions from one another, at $B_{eff}(H_{dec}) = B_{eff}(H_{inc})$ we obtain

$$\Delta H = 4\pi\alpha\{M(H_{dec}) - M(H_{inc})\}. \quad (4)$$

As we mentioned above, it is assumed here that the parameter α is independent of the external field. Then, the identity of the behavior of ΔH versus H_{dec} at different temperatures for different samples can be explained by the approximately identical behavior of

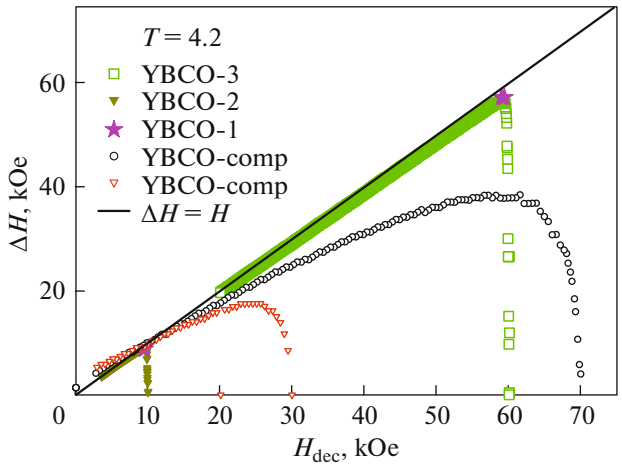

Fig. 10. Magnetoresistance hysteresis field width ΔH versus H_{dec} for the investigated samples (symbols) at T = 4.2 K (the H_{max} values are different). The solid line shows the linear dependence $\Delta H = H_{dec}$.

the magnetization hysteresis, as well as its temperature evolution. On the other hand, the parameter α is fairly large and apparently almost temperature-independent [67–69, 79]. Therefore, the discovered universal behavior of the magnetoresistance hysteresis width illustrated in Fig. 9 can be qualitatively explained. The parameter α determines, in fact, the effective crowding of the magnetic induction lines from the magnetic moments of grains in the region of a grain boundary. As is known, the length of grain boundaries in the yttrium HTS system is extremely small and, naturally, the large J_C values correspond to the grain boundaries with the smallest length (thickness l) [3–6]. In [6], we estimated the l values for different yttrium HTS samples by comparing the experimental and theoretical [80] temperature dependences of the critical current at $H = 0$. For the best samples (J_C (T = 4.2 K) ~ 1.4 kA/cm^2), the l value was merely ~1/10 of the coherence length ξ_0, while for the sample with the J_C value smaller by an order of magnitude, thickness l increased to ~1ξ_0. For a series of samples YBCO-1, 2, 3, it is natural that a decrease in J_C (Table 1) will correspond to an increase in the grain boundary thickness. Such an increase in the thickness of intergrain spacers should affect the α value; however, the established identity of the behavior of the $R(H)$ hysteresis width indicates approximately the same degree of magnetic flux crowding. Possibly, when an external field is applied, an additional effect arises, when the field (the effective field is meant) and a part of the surface region of HTS grains already behave as an intergrain spacer. Then, we can expect approximately the same degree of flux crowding in the intergrain medium for the investigated series of samples with different current-carrying capacities.

The above-described feature consisting in the identical behavior of the $R(H)$ hysteresis width for different granular samples is not observed in the composite sample. Figure 10 shows the $\Delta H(H_{dec})$ data for samples YBCO-1, 2, 3 and YBCO-comp at a temperature of 4.2 K. It can be seen that the data for the composite can no longer be described, even approximately, by a linear scaling function; moreover, the $\Delta H(H_{dec})$ dependence for this sample is located much lower than for samples YBCO-1, 2, 3. Here, according to Eq. (4), we can already speak about the weaker flux compression in the region of intergrain boundaries than in pure YBCO. It is clear that the thickness of the boundaries between HTS grains in the composite sample significantly increased.[2] The estimation of the effective thickness for the composites with metal oxide $BaPbO_3$ obtained by a similar technique and the content of a nonsuperconducting component yielded a d value of about 3ξ_0 [6]. Consequently, for the composite, it is reasonable to expect a lower degree of the flux compression or the smaller α value, which can be seen in Fig. 10 from the $\Delta H(H_{dec})$ data.

4. CONCLUSIONS

The magnetoresistance hysteresis in granular HTSs is driven by the dissipation processes in grain boundaries; in this case, in the intergrain spacings, one should consider the effective field B_{eff} rather than the external field. This effective field is a superposition of the external field and the field induced by the magnetic response of HTS grains. Consequently, the magnetic hysteresis of granular HTSs determines their magnetotransport hysteresis.

The main result of this study can be considered the discovered universal behavior of the magnetoresistance hysteresis width $\Delta H = H_{dec} - H_{inc}$ (under the condition $R(H_{dec}) = R(H_{inc})$) of the Y–Ba–Cu–O granular HTSs. In a fairly wide external field range, the ΔH parameter has a functional dependence close to linear and this dependence is the same both at the temperatures close to critical (above 77 K) and at low temperatures (T = 4.2 K). Moreover, the data turned out to be identical for three samples with different critical transport current densities, from the high (1.5 kA/cm^2 at 4.2 K) to fairly low (100 A/cm^2 at 4.2 K) J_C values. The reason for such a universal behavior independent of the quality of grain boundaries is the magnetic flux compression in the intergrain medium. The degree of the flux compression is apparently approximately the same for the samples with different current-carrying capacities. However, an exception is the HTS composite, in which the critical current is even stronger suppressed (J_C ~ 0.1 A/cm^2 at

[2] The effective thickness of the boundaries between HTS grains in the composite depends on the concentration of a nonsuperconducting component [6, 23, 53, 72].

4.2 K) due to the fact that the non-superconducting component (in this case, CuO) acts as spacers between grains and, as a result, the effective length of boundaries in the composite becomes much larger than the length of natural boundaries in pure Y–Ba–Cu–O. For such a composite sample, the effect of flux compression in the intergrain medium works to a lesser extent. Thus, the sufficiently strong flux compression in the region of grain boundaries is the main reason for the observed broad magnetoresistance hysteresis, which determines the universal behavior of the width of this hysteresis for the yttrium HTS samples.

ACKNOWLEDGMENTS

The authors are grateful to D.M. Gokhfeld for discussion of the results. The measurements of the transport properties were performed in part on a PPMS-6000 system of the Center for Collective Use, Krasnoyarsk Scientific Center, Siberian Branch of the Russian Academy of Sciences.

CONFLICT OF INTEREST

The authors declare that they have no conflicts of interest.

REFERENCES

1. L. Ji, M. S. Rzchowski, N. Anand, and M. Tinkham, Phys. Rev. B **47**, 470 (1993).
2. M. Prester, Supercond. Sci. Technol. **11**, 333 (1998).
3. M. I. Petrov, D. A. Balaev, B. P. Khrustalev, and K. S. Aleksandrov, Phys. C (Amsterdam, Neth.) **235–240**, 3043 (1994).
4. R. Gross, Phys. C (Amsterdam, Neth.) **432**, 105 (2005).
5. J. Mannhart, Phys. C (Amsterdam, Neth.) **450**, 152 (2006).
6. M. I. Petrov, D. A. Balaev, and D. M. Gokhfel'd, Phys. Solid State **49**, 619 (2007).
7. J. H. Durrell and N. A. Rutter, Supercond. Sci. Technol. **22**, 013001 (2009).
8. X. Obradors, T. Puig, S. Ricart, M. Coll, J. Gazquez, A. Palau, and X. Granados, Supercond. Sci. Technol. **25**, 123001 (2012).
9. G. Wang, M. J. Raine, and D. P. Hampshire, Supercond. Sci. Technol. **30**, 104001 (2017).
10. R. J. Joshi, R. B. Hallock, and J. A. Taylor, Phys. Rev. B **55**, 9107 (1997).
11. J. W. C. de Vries, G. M. Stollman, and M. A. M. Gijs, Phys. C (Amsterdam, Neth.) **157**, 406 (1989).
12. A. C. Wright, K. Zhang, and A. Erbil, Phys. Rev. B **44**, 863 (1991).
13. C. Ganey, H. Petersen, and R. Bednar, Phys. Rev. B **48**, 3388 (1993).
14. H. S. Gamchi, G. J. Russell, and K. N. R. Taylor, Phys. Rev. B **50**, 12950 (1994).
15. R. J. Soulen, T. L. Francavilla, W. W. Fuller-Mora, M. M. Miller, C. H. Joshi, W. L. Carter, A. J. Rodenbush, M. D. Manlief, and D. Aized, Phys. Rev. B **50**, 478 (1994).
16. D. H. Liebenberg, R. J. Soulen, T. L. Francavilla, W. W. Fuller-Mora, P. C. McIntyre, and M. J. Cima, Phys. Rev. B **51**, 11838 (1995).
17. R. J. Soulen, T. L. Francavilla, A. R. Drews, L. Toth, M. S. Osofsly, W. L. Lechter, and E. F. Skelton, Phys. Rev. B **51**, 1393 (1995).
18. W. M. Tieran, R. Joshi, and R. B. Hallock, Phys. Rev. B **48**, 3423 (1993).
19. Y. Zhao, X. B. Zuge, J. M. Xu, and L. Cao, Phys. Rev. B **49**, 6985 (1994).
20. L. Urba, C. Acha, and V. Bekeris, Phys. C (Amsterdam, Neth.) **279**, 95 (1997).
21. H. Shakeripour and M. Akhavan, Supercond. Sci. Technol. **14**, 234 (2001).
22. M. R. Mohammadizadeh and M. Akhavan, Supercond. Sci. Technol. **16**, 538 (2003).
23. D. A. Balaev, S. I. Popkov, K. A. Shaikhutdinov, and M. I. Petrov, Phys. Solid State **48**, 826 (2006).
24. M. A. Vasyutin, Tech. Phys. Lett. **39**, 1078 (2013).
25. V. V. Derevyanko, T. V. Sukhareva, and V. A. Finkel', Phys. Solid State **60**, 470 (2018).
26. T. V. Sukhareva and V. A. Finkel, JETP Lett. **108**, 243 (2018).
27. T. V. Sukhareva and V. A. Finkel, J. Low Temp. Phys. **44**, 194 (2018).
28. T. V. Sukhareva and V. A. Finkel, J. Low Temp. Phys. **46**, 550 (2020).
29. S. Shifang, Z. Yong, P. Guoqian, Y. Daoq, Z. An, C. Zuyao, Q. Yitai, K. Eiyan, and Z. Qirui, Europhys. Lett. **6**, 359 (1988).
30. Y. J. Quian, Z. M. Tang, K. Y. Chen, B. Zhou, J. W. Qui, B. C. Miao, and Y. M. Cai, Phys. Rev. B **39**, 4701 (1989).
31. P. Mune, F. C. Fonseca, R. Muccillo, and R. F. Jardim, Phys. C (Amsterdam, Neth.) **390**, 363 (2003).
32. N. D. Kuz'michev, JETP Lett. **74**, 262 (2001).
33. N. D. Kuz'michev, Phys. Solid State **43**, 2012 (2001).
34. I. Felner, E. Galstyan, B. Lorenz, D. Cao, Y. S. Wang, Y. Y. Xue, and C. W. Chu, Phys. Rev. B **167**, 134506 (2003).
35. T. V. Sukhareva and V. A. Finkel, J. Exp. Theor. Phys. **107**, 787 (2008).
36. T. V. Sukhareva and V. A. Finkel', Phys. Solid State **50**, 1001 (2008).
37. V. V. Derevyanko, T. V. Sukhareva, and V. A. Finkel', Tech. Phys. **53**, 321 (2008).
38. T. V. Sukhareva and V. A. Finkel', Phys. Solid State **52**, 452 (2010).
39. K. A. Shaikhutdinov, D. A. Balaev, S. I. Popkov, and M. I. Petrov, Phys. Solid State **51**, 1105 (2009).
40. D. A. Balaev, S. I. Popkov, S. V. Semenov, A. A. Bykov, K. A. Shaykhutdinov, D. M. Gokhfeld, and M. I. Petrov, Phys. C (Amsterdam, Neth.) **470**, 61 (2010).
41. A. Altinkok, K. Kilic, M. Olutas, and A. Kilic, J. Supercond. Nov. Magn. **26**, 3085 (2013).
42. D. A. Balaev, S. I. Popkov, K. A. Shaikhutdinov, M. I. Petrov, and D. M. Gokhfeld, Phys. Solid State **56**, 1542 (2014).
43. J. E. Evetts and B. A. Glowacki, Cryogenics **28**, 641 (1988).

44. M. E. McHenry, P. P. Maley, and J. O. Willis, Phys. Rev. B **40**, 2666 (1989).
45. E. Altshuler, J. Musa, J. Barroso, A. R. R. Papa, and V. Venegas, Cryogenics **33**, 308 (1993).
46. P. Mune, E. Govea-Alcaide, and R. F. Jardim, Phys. C (Amsterdam, Neth.) **354**, 275 (2001).
47. D. A. Balaev, A. A. Dubrovskii, S. I. Popkov, D. M. Gokhfeld, S. V. Semenov, K. A. Shaikhutdinov, and M. I. Petrov, Phys. Solid State **54**, 2155 (2012).
48. D. López and F. de la Cruz, Phys. Rev. B **43**, 11478 (1991).
49. D. López, R. Decca, and F. de la Cruz, Supercond. Sci. Technol. **5**, S276 (1992).
50. O. V. Gerashchenko and S. L. Ginzburg, Supercond. Sci. Technol. **13**, 332 (2000).
51. A. Kilic, K. Kilic, S. Senoussi, and K. Demir, Phys. C (Amsterdam, Neth.) **294**, 203 (1998).
52. D. Daghero, P. Mazzetti, A. Stepanescu, and P. Tura, Phys. Rev. B **66**, 11478 (2002).
53. D. A. Balaev, A. G. Prus, K. A. Shaykhutdinov, D. M. Gokhfeld, and M. I. Petrov, Supercond. Sci. Technol. **20**, 495 (2007).
54. S. V. Semenov, D. A. Balaev, M. A. Pochekutov, and D. A. Velikanov, Phys. Solid State **59**, 1291 (2017).
55. D. A. Balaev, S. V. Semenov, and M. A. Pochekutov, J. Appl. Phys. **122**, 123902 (2017).
56. A. V. Mitin, Phys. C (Amsterdam, Neth.) **235–240**, 3311 (1994).
57. V. V. Derevyanko, T. V. Sukhareva, and V. A. Finkel', Phys. Solid State **46**, 1798 (2004).
58. V. V. Derevyanko, T. V. Sukhareva, and V. A. Finkel', Phys. Solid State **49**, 1829 (2007).
59. T. V. Sukhareva and V. A. Finkel, Phys. Solid State **53**, 914 (2011).
60. D. A. Balaev, A. A. Bykov, S. V. Semenov, S. I. Popkov, A. A. Dubrovskii, K. A. Shaikhutdinov, and M. I. Petrov, Phys. Solid State **53**, 922 (2011).
61. D. A. Balaev, S. V. Semenov, and M. I. Petrov, Phys. Solid State **55**, 2422 (2013).
62. V. V. Derevyanko, T. V. Sukhareva, V. A. Finkel, and Yu. N. Shakhov, Phys. Solid State **56**, 649 (2014).
63. D. A. Balaev, D. M. Gokhfeld, A. A. Dubrovski, S. I. Popkov, K. A. Shaikhutdinov, and M. I. Petrov, J. Exp. Theor. Phys. **105**, 1174 (2007).
64. D. A. Balaev, A. A. Dubrovskii, K. A. Shaikhutdinov, S. I. Popkov, D. M. Gokhfeld, Yu. S. Gokhfeld, and M. I. Petrov, J. Exp. Theor. Phys. **108**, 241 (2009).
65. D. A. Balaev, S. I. Popkov, E. I. Sabitova, S. V. Semenov, K. A. Shaykhutdinov, A. V. Shabanov, and M. I. Petrov, J. Appl. Phys. **110**, 093918 (2011).
66. D. A. Balaev, S. V. Semenov, and M. I. Petrov, J. Supercond. Nov. Magn. **27**, 1425 (2014).
67. S. V. Semenov and D. A. Balaev, Phys. C (Amsterdam, Neth.) **550**, 19 (2018).
68. S. V. Semenov and D. A. Balaev, J. Supercond. Nov. Magn. **32**, 2409 (2019).
69. S. V. Semenov and D. A. Balaev, Phys. Solid State **62**, 1136 (2020).
70. S. V. Semenov, A. D. Balaev, and D. A. Balaev, J. Appl. Phys. **125**, 033903 (2019).
71. G. Blatter, M. V. Feigel'man, V. B. Gekshkebein, A. I. Larkin, and V. M. Vinokur, Rev. Mod. Phys. **66**, 1125 (1994).
72. M. I. Petrov, D. A. Balaev, K. A. Shaihutdinov, and K. S. Aleksandrov, Supercond. Sci. Technol. **14**, 798 (2001).
73. D. M. Gokhfeld, Phys. Solid State **56**, 2380 (2014).
74. D. M. Gokhfel'd, Tech. Phys. Lett. **45**, 1 (2019).
75. C. P. Bean, Rev. Mod. Phys. **36**, 31 (1964).
76. C. A. M. dos Santos, M. S. da Luz, B. Ferreira, and A. J. S. Machado, Phys. C (Amsterdam, Neth.) **391**, 345 (2003).
77. D. A. Balaev, S. I. Popkov, S. V. Semenov, A. A. Bykov, E. I. Sabitova, A. A. Dubrovskiy, K. A. Shaikhutdinov, and M. I. Petrov, J. Supercond. Nov. Magn. **24**, 2129 (2011).
78. V. V. Derevyanko, T. V. Sukhareva, and V. A. Finkel', Phys. Solid State **59**, 1492 (2017).
79. D. A. Balaev, S. V. Semenov, and D. M. Gokhfeld, J. Supercond. Nov. Magn. (2021, in press). https://doi.org/10.1007/s10948-021-05812-2
80. U. Gunsenheimer, U. Schussler, and R. Kümmel, Phys. Rev. B **49**, 6111 (1994).

Translated by E. Bondareva